Calculations of Electron Inelastic Mean Free Paths

II. Data for 27 Elements over the 50–2000 eV Range

S. Tanuma

Analysis Research Center, Nippon Mining Company Ltd., 3-17-35 Niizo-Minami, Toda, Saitama 335, Japan

C. J. Powell and D. R. Penn

National Institute of Standards and Technology, Gaithersburg, MD 20899, USA

We report calculations of electron inelastic mean free paths (IMFPs) for 50–2000 eV electrons in a group of 27 elements (C, Mg, Al, Si, Ti, V, Cr, Fe, Ni, Cu, Y, Zr, Nb, Mo, Ru, Rh, Pd, Ag, Hf, Ta, W, Re, Os, Ir, Pt, Au and Bi). This work extends our previous calculations (*Surf. Interface Anal.* 11, 577 (1988)) for the 200–2000 eV range. Substantial variations were found in the shapes of the IMFP versus energy curves from element to element over the 50–200 eV range and we attribute these variations to the different inelastic scattering properties of each material. Our calculated IMFPs were fitted to a modified form of the Bethe equation for inelastic electron scattering in matter; this equation has four parameters. These four parameters could be empirically related to several material parameters for our group of elements (atomic weight, bulk density and number of valence electron per atom). IMFPs were calculated from these empirical expressions and we found that the root mean square difference between these IMFPs and those initially calculated was 13%. The modified Bethe equation and our expressions for the four parameters can therefore be used to estimate IMFPs in other materials. The uncertainties in the algorithm used for our IMFP calculation are difficult to estimate but are believed to be largely systematic. Since the same algorithm has been used for calculating IMFPs, our predictive IMFP formula is considered to be particularly useful for predicting the IMFP dependence on energy in the 50–2000 eV range and the material dependence for a given energy.

INTRODUCTION

In a previous paper, we reported new calculations of electron inelastic mean free paths (IMFPs) for 200–2000 eV electrons in 27 elements and four compounds.[1] These calculations were based on an algorithm developed by Penn,[2] which makes use of experimental optical data (to represent the dependence of the inelastic scattering probability on energy loss) and the theoretical Lindhard dielectric function (to represent the dependence of the scattering probability on momentum transfer). We fitted the calculated IMFPs to the Bethe equation for inelastic electron scattering in matter[3] and the two parameters in the Bethe equation were empirically related to several material constants. The resulting formula, to be referred to as TPP-1, could be used for predicting the IMFP dependence on electron energy for a given material and the material dependence for a given energy.

We extend the earlier work in the present paper by reporting IMFP calculations for the same 27 elements over the energy range 50–2000 eV. We use the same algorithm as that employed earlier but here we do not make an approximation adopted previously that is only valid for energies greater than 200 eV. The IMFP values have been fitted to a modified form of the Bethe equation with four parameters; these four parameters have again been empirically related to material constants. We thus obtained a new formula, to be referred to as TPP-2, for predicting IMFP values over the 50–2000 eV range. Preliminary accounts of this work have

been published.[4,5] Results of similar IMFP calculations for 15 compounds are presented in a separate paper.[6]

Values of electron attenuation lengths (ALs) are needed for quantitative surface analyses by AES and XPS over the typical electron energy range of 50–2000 eV. Jablonski,[7] however, has recently found that IMFP values rather than ALs are appropriate for AES under some conditions.

We present below our IMFP results for 27 elements (C, Mg, Al, Si, Ti, V, Cr, Fe, Ni, Cu, Y, Zr, Nb, Mo, Ru, Rh, Pd, Ag, Hf, Ta, W, Re, Os, Ir, Pt, Au and Bi). These elements were selected since the optical data needed for the calculation were conveniently available.[1] We then give an analysis of the energy dependence of the IMFPs over the 50–2000 eV energy range and show how we developed the predictive formula TPP-2. The limitations of this formula and the sensitivity of the computed IMFPs to the choice of parameters are discussed. Finally, we show that the different shapes of the IMFP versus energy curves at energies below 200 eV are associated with the different inelastic electron scattering properties of the materials.

IMFP CALCULATION

Our previous paper[1] summarizes the method of IMFP calculation. Briefly, it is assumed that the material of interest can be considered to be a uniform electron gas that can be characterized by a complex dielectric constant $\varepsilon(q, \omega)$, where q is the momentum transfer and ω is

the frequency corresponding to an energy transfer $\hbar\omega$ in an inelastic scattering event. We have made use of the Lindhard dielectric function[8] in our model expression for $\varepsilon(q, \omega)$ and equate our model dielectric function for $q = 0$ with experimental measurements of $\varepsilon(\omega)$. For electron energies between 50 and 200 eV, the IMFP is calculated from Eqn. (14) of Ref. 1, which involves a triple integration over q, ω and an electron density variable in the Lindhard expression. The final integration represents a weighted average over all electron densities, where the weighting is determined by the experimental optical data in accordance with Eqn. (9) of Ref. 1. For energies above 200 eV, we calculated IMFPs from Eqn. (16) of Ref. 1, which requires only a single integration over excitation energy. Electron energies are expressed with respect to the Fermi level.

The IMFP calculation for each element is based on experimental data for $\varepsilon(\omega)$. For over half of the materials, there were gaps in the tabulations[9-12] of optical constants, often in the photon energy range 40–100 eV; in such cases, we made interpolations based on atomic photoabsorption calculations.[13] The accuracy of the experimental $\varepsilon(\omega)$ was tested previously with two useful sum rules.[1] This analysis indicated that the root mean square (RMS) uncertainty of the optical data was $\sim 10\%$.

The IMFPs calculated at low energies (< 100 eV) are subject to much greater uncertainties than those at higher energies. For low energies, it is not clear if the Born approximation is valid, i.e. whether or not the screened electron–electron interaction is properly treated in lowest-order perturbation theory. Furthermore, the effects of exchange and correlation have been neglected and these are expected to have a strong influence at low energies. Ashley[14] has found an increase in IMFP values at low energies when exchange was treated in an approximate way. Unfortunately, it is not presently clear how to take exchange and correlation into account in a first-principles calculation of the dielectric function. These effects could increase the IMFP because the electron–electron interaction is weakened on account of electrons seeking to avoid each other. However, another plausible treatment[15] of these effects has yielded shorter IMFPs. More accurate assessments of correlation and exchange effects remain to be made.

Our assumption that the material can be considered as a free-electron gas is not expected to be valid for non-free-electron-like materials, such as the transition and noble metals. Nevertheless, our use of experimental optical data ensures that we correctly represent the excitation spectrum of each material, i.e. we do not assume that plasmon excitation is the only or the dominant excitation channel. The free-electron-gas approximation enables us to apply the Lindhard dielectric formalism, which provides a physically plausible dependence of the dielectric constant on momentum transfer. This particular dependence may not be valid for non-free-electron-like materials but we do not currently have better theoretical or experimental guidance. At low energies, the actual band structure of a solid should be taken into account in an IMFP calculation if it differs significantly from that of a free-electron-like material. For example, transition metals have unfilled d bands and large densities of states above the Fermi energy. There is some

evidence[16] that experimental ALs are much smaller than expected from this and similar IMFP calculations.

We note finally here that our IMFP calculations are for bulk solids. At surfaces, there are additional complications (e.g. the excitation of surface plasmons) that affect both IMFP calculations and AL measurements.[17] For electron energies below ~ 200 eV in free-electron-like solids, surface plasmon excitation becomes comparable to or larger than bulk plasmon excitation in reflection electron energy-loss experiments.[18] In such experiments, the detected electrons cross the solid–vacuum interface twice whereas the detected electrons in AES and XPS experiments cross this interface once and the surface plasmon loss intensity is smaller than in the corresponding energy-loss experiments; the surface plasmon intensity also depends on the experimental geometry.[19] The rise in the surface plasmon intensity in the energy-loss experiments is accompanied by a similar but not identical decrease in the bulk plasmon intensity. As a result, the total inelastic scattering cross-section is not greatly modified by the changes in the relative cross-sections for bulk plasmon and surface plasmon excitations except perhaps at near-grazing take-off angles.[19]

To summarize, we expect our IMFP calculations to be useful for electron energies greater than about 50 eV. The uncertainties in the calculated IMFPs at low energies (50–200 eV) will be greater than at higher energies but it is not possible for us to estimate these uncertainties reliably. Since we are using the same algorithm to calculate IMFPs for a large number of materials, we believe that we can determine IMFP variations with higher accuracy than the IMFP values themselves. We also can similarly analyse the dependence of the IMFP on electron energy with high precision.

IMFP RESULTS

In the present work, we used values for the Fermi energy (Table 1) from band structure calculations[20,21] rather than from the formula for a free-electron gas. As a result, our IMFP values for electron energies between 50 and 2000 eV (Table 2) are typically $\sim 0.1–0.2$ Å larger than the values presented earlier[1] for the 200–2000 eV range. The IMFP values for Ir are 10–20% smaller than found previously owing to the use of a less accurate algorithm for numerical integration in one of our early calculations.

Plots of IMFP versus energy are shown in Figs 1–10 for C, Si, Ti, Fe, Mo, Pd, Ag, W, Pt and Bi; the insets in each figure show the new results for low energies (< 200 eV) on an expanded energy scale. The insets also show IMFP values that were calculated for energies between 10 and 40 eV; these values are included to indicate the trends for energies below the IMFP minimum but we emphasize, for the reasons presented earlier, that these values should be regarded only as rough estimates. Plots similar to Figs 1–10 for Mg, Al, Ni, Cu and Au are given in our previous publications.[4,5] These plots show the qualitative differences in the shapes of the IMFP versus energy variations at low energy that was discussed previously.[5]

Table 1. Values of the Fermi energy used in our IMFP calculations (Refs 18 and 19) and of the free-electron plasmon energies for the group of 27 elements[a]

Element	Fermi energy (eV)	Plasmon energy (eV)
C	20.4	22.3
Mg	7.1	10.9
Al	11.2	15.8
Si	12.5	16.6
Ti	6.0	17.7
V	6.4	22.3
Cr	7.8	26.2
Fe	8.9	30.6
Ni	9.1	35.5
Cu	8.7	35.9
Y	4.4	11.2
Zr	5.2	15.4
Nb	5.3	19.5
Mo	6.5	23.0
Ru	6.9	28.5
Rh	6.9	30.0
Pd	6.2	30.6
Ag	7.2	29.8
Hf	7.9	15.7
Ta	8.4	19.5
W	10.1	22.9
Re	10.7	25.6
Os	11.4	28.1
Ir	11.2	29.5
Pt	10.6	30.2
Au	9.0	29.9
Bi	12.6	13.9

[a] The free-electron plasmon energies have been calculated using the values of N_v shown in Table 3 of Ref. 1; for Bi, $N_v = 5$ was assumed here.

Figure 2. IMFP results for silicon as a function of electron energy; see caption to Fig. 1.

Figure 3. IMFP results for titanium as a function of electron energy; see caption to Fig. 1.
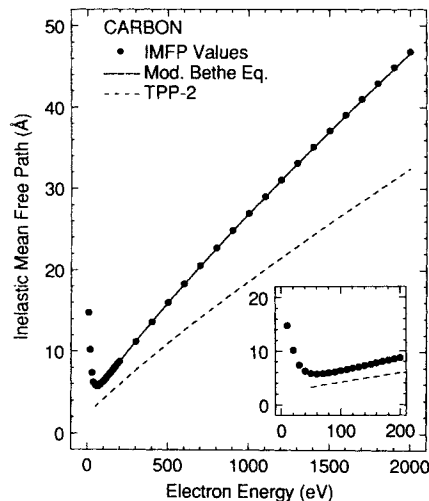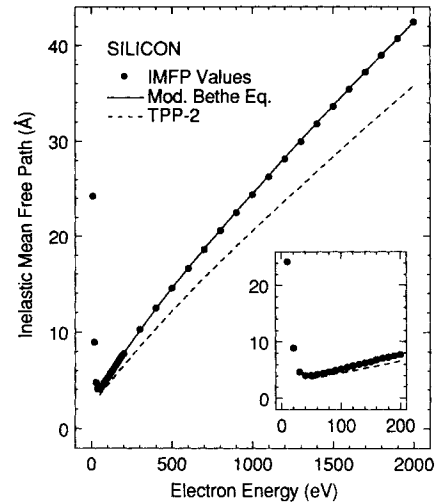

Figure 1. IMFP values (solid circles) calculated for glassy carbon (Table 2) as a function of electron energy. IMFP values are shown for 10–40 eV electrons to illustrate trends but these results are not considered to be reliable (see text). The solid line is a fit to the IMFP values with the modified Bethe equation (Eqn. (2)); values of the parameters found in the fit are listed in Table 3. The dashed line shows IMFP values calculated from our predictive formula TPP-2 (Eqn. (2)), where values of the four parameters were calculated from property data for carbon using (Eqn. (3)). The inset shows the low-energy region on an expanded energy scale.

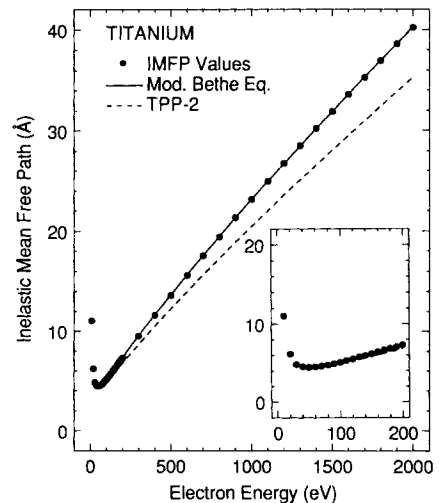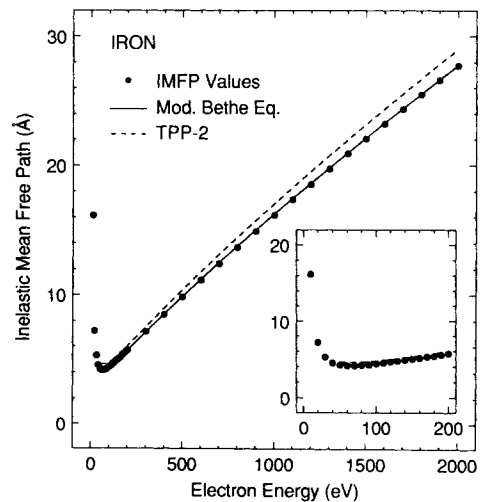Figure 4. IMFP results for iron as a function of electron energy; see caption to Fig. 1.

Table 2. Calculated IMFPs as a function of electron energy for 27 elements

Electron energy (eV)	C[a]	Mg	Al	Si	Ti	V	Cr	Fe	Ni	Cu	Y	Zr	Hb	Mo
50	5.9	4.0	3.2	4.1	4.5	4.2	4.4	4.3	4.9	5.0	5.0	4.4	6.0	5.1
100	6.4	5.4	4.2	5.3	5.1	4.9	4.3	4.4	4.6	5.0	5.5	4.8	6.0	4.5
150	7.5	6.8	5.3	6.5	6.2	5.9	5.0	5.1	5.1	5.6	6.4	5.7	6.7	5.0
200	8.8	8.2	6.3	7.8	7.3	6.8	5.7	5.8	5.7	6.2	7.5	6.6	7.7	5.6
300	11.2	10.7	8.3	10.3	9.5	8.8	7.2	7.2	6.9	7.7	9.8	8.6	9.7	7.1
400	13.7	13.0	10.0	12.5	11.6	10.7	8.6	8.5	8.1	9.0	11.9	10.5	11.7	8.5
500	16.0	15.3	11.7	14.6	13.7	12.5	10.0	9.8	9.2	10.2	14.0	12.3	13.7	10.0
600	18.4	17.5	13.3	16.6	15.6	14.3	11.4	11.2	10.4	11.4	16.0	14.1	15.6	11.3
700	20.6	19.6	14.9	18.6	17.6	16.0	12.7	12.4	11.5	12.7	17.9	15.8	17.4	12.7
800	22.8	21.7	16.5	20.6	19.5	17.7	14.0	13.7	12.7	13.9	19.8	17.5	19.2	14.0
900	24.9	23.8	18.1	22.5	21.3	19.4	15.3	14.9	13.8	15.1	21.6	19.1	20.9	15.2
1000	27.0	25.9	19.6	24.4	23.2	21.0	16.6	16.2	14.9	16.3	23.4	20.7	22.6	16.5
1100	29.1	27.9	21.1	26.3	25.0	22.7	17.9	17.4	16.0	17.5	25.2	22.3	24.3	17.7
1200	31.1	29.9	22.6	28.2	26.8	24.3	19.1	18.6	17.0	18.7	27.0	23.8	25.9	18.9
1300	33.1	31.9	24.1	30.0	28.5	25.9	20.4	19.8	18.1	19.8	28.7	25.4	27.5	20.1
1400	35.2	33.9	25.5	31.8	30.2	27.4	21.6	20.9	19.2	21.0	30.4	26.9	29.1	21.2
1500	37.1	35.8	27.0	33.7	31.9	29.0	22.8	22.1	20.2	22.1	32.1	28.4	30.7	22.4
1600	39.1	37.7	28.4	35.4	33.6	30.5	24.0	23.2	21.2	23.3	33.8	29.9	32.3	23.5
1700	41.1	39.7	29.9	37.2	35.3	32.0	25.1	24.4	22.3	24.4	35.5	31.3	33.8	24.7
1800	43.0	41.6	31.3	39.0	36.9	33.5	26.3	25.5	23.3	25.5	37.1	32.8	35.3	25.8
1900	44.9	43.5	32.7	40.7	38.6	34.9	27.5	26.6	24.3	26.6	38.8	34.2	36.9	26.9
2000	46.8	45.3	34.1	42.5	40.2	36.4	28.6	27.7	25.3	27.7	40.4	35.7	38.4	28.0

	Ru	Rh	Pd	Ag	Hf	Ta	W	Re	Os	Ir	Pt	Au	Bi
50	4.9	4.8	4.8	6.2	5.8	4.8	5.0	5.2	5.5	5.3	5.0	6.7	4.9
100	4.2	4.1	4.8	4.9	6.2	4.5	4.1	3.8	4.3	4.3	4.2	4.8	5.5
150	4.6	4.5	5.4	5.0	7.1	5.0	4.5	3.9	4.5	4.7	4.5	4.8	6.3
200	5.2	5.0	6.2	5.5	8.0	5.5	5.0	4.3	5.0	5.2	4.9	5.1	7.2
300	6.5	6.1	7.8	6.4	10.2	6.8	6.1	5.1	6.0	6.4	6.0	6.0	8.8
400	7.8	7.3	9.4	7.6	12.0	8.0	7.3	6.0	7.1	7.5	7.1	7.1	10.6
500	9.1	8.5	11.0	8.7	13.8	9.2	8.4	6.9	8.1	8.7	8.2	8.1	12.3
600	10.4	9.7	12.5	9.9	15.6	10.4	9.4	7.7	9.1	9.7	9.2	9.1	14.0
700	11.6	10.8	14.0	11.0	17.3	11.5	10.4	8.5	10.1	10.8	10.2	10.1	15.6
800	12.8	12.0	15.4	12.1	19.0	12.7	11.4	9.4	11.1	11.8	11.2	11.1	17.2
900	14.0	13.0	16.8	13.2	20.6	13.7	12.4	10.1	12.0	12.8	12.2	12.0	18.7
1000	15.1	14.1	18.2	14.2	22.2	14.8	13.4	10.9	12.9	13.8	13.1	12.9	20.2
1100	16.3	15.1	19.6	15.3	23.8	15.9	14.3	11.7	13.8	14.7	14.0	13.9	21.7
1200	17.4	16.2	20.9	16.3	25.3	16.9	15.2	12.5	14.7	15.7	14.9	14.8	23.2
1300	18.5	17.2	22.2	17.3	26.9	17.9	16.2	13.2	15.6	16.6	15.8	15.7	24.6
1400	19.5	18.2	23.5	18.3	28.4	19.0	17.1	14.0	16.4	17.6	16.7	16.5	26.1
1500	20.6	19.2	24.7	19.2	29.9	20.0	18.0	14.7	17.3	18.5	17.6	17.4	27.5
1600	21.6	20.1	26.0	20.2	31.4	21.0	18.9	15.4	18.1	19.4	18.5	18.3	28.9
1700	22.7	21.1	27.2	21.1	32.9	22.0	19.8	16.2	19.0	20.3	19.3	19.1	30.3
1800	23.7	22.0	28.4	22.1	34.4	22.9	20.6	16.9	19.8	21.2	20.2	20.0	31.6
1900	24.7	23.0	29.7	23.0	35.8	23.9	21.5	17.6	20.7	22.1	21.1	20.8	33.0
2000	25.7	23.9	30.9	24.0	37.3	24.9	22.4	18.3	21.5	22.9	21.9	21.6	34.4

[a] Glassy form.

IMFP dependence on electron energy

We found in our analysis of IMFPs for 200–2000 eV electrons that the Bethe equation[3] for inelastic scattering in matter provided a satisfactory description of the IMFP dependence on energy.[1] This equation has also proved to be useful in analysing inner-shell ionization cross-sections,[22] other IMFP calculations[23] and measurements of electron attenuation lengths (ALs).[24]

The Bethe equation can be written

$$\lambda = E/[E_p^2 \beta \ln(\gamma E)] \tag{1}$$

where λ is the IMFP (in Å), E is the electron energy (in eV), $E_p = 28.8 \, (N_v \rho/M)^{1/2}$ is the free-electron plasmon energy (in eV), ρ is the bulk density (in g cm^{-3}), N_v is the number of valence electrons per atom or molecule, M is the atomic or molecular weight and β and γ are parameters. Values of the plasmon energy for the 27 elements are listed in Table 1. The validity of the Bethe equation for a particular set of IMFP or AL data can be readily checked using a Fano plot in which (E/λ) is plotted versus ln E. [23,24] If the data points lie sufficiently close to a straight line, values of the parameters β and γ in Eqn. (1) can be found through a linear least-squares analysis.

In our present work, it has been necessary to modify the Bethe equation through the addition of two terms (as proposed by Inokuti[25] and Ashley[14])

$$\lambda = E/\{E_p^2[\beta \ln(\gamma E) - (C/E) + (D/E^2)]\} \tag{2}$$
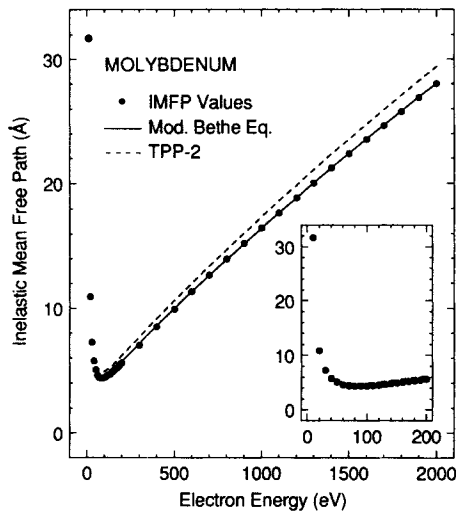
Figure 5. IMFP results for molybdenum as a function of electron energy; see caption to Fig. 1.
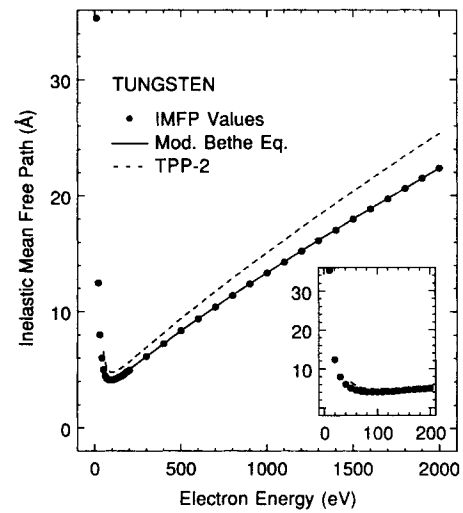

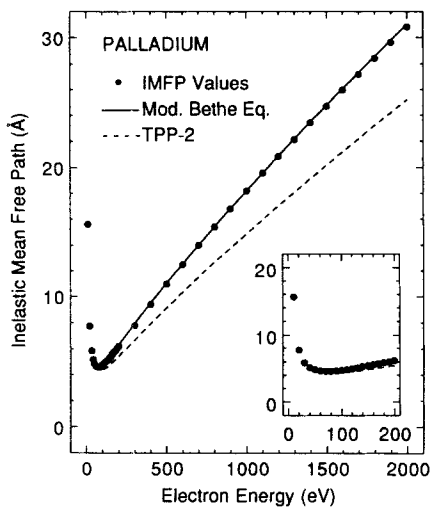**Figure 8.** IMFP results for tungsten as a function of electron energy; see caption to Fig. 1.

Figure 6. IMFP results for palladium as a function of electron energy; see caption to Fig. 1.
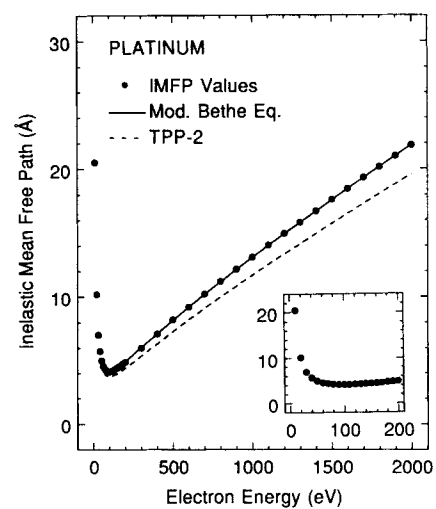

Figure 9. IMFP results for platinum as a function of electron energy; see caption to Fig. 1.
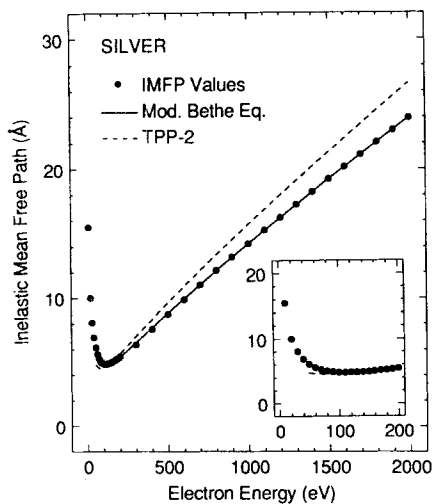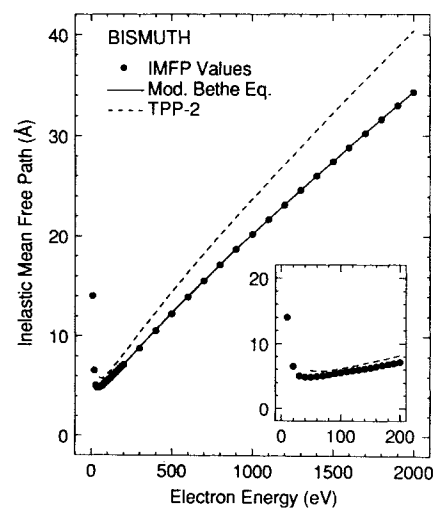

Figure 7. IMFP results for silver as a function of electron energy; see caption to Fig. 1.

Figure 10. IMFP results for bismuth as a function of electron energy; see caption to Fig. 1.

where C and D are two additional parameters. The added terms in Eqn. (2) account in an empirical way for exchange effects expected to be significant at low energies and for other departures from the first Born approximation on which the Bethe formula is based.[25]

The need for the additional terms in Eqn. (2) can be seen from the Fano plots based on our IMFP results for Si and Pt shown in Figs 11 and 12. The Fano plots for these two elements are shown as examples of the different dependences of λ versus E at low energies illustrated in Figs 1–10. For Si, the calculated IMFP (Fig. 2) decreases rapidly with increasing energy to a well-defined minimum at ~ 40 eV and then increases; in contrast, the calculated IMFP for Pt (Fig. 9) decreases more gradually and there is a broader minimum located at ~ 100 eV. The Fano plot for Si in Fig. 11 shows departures from linearity for energies below ~ 200 eV, while for Pt the departures from linearity in Fig. 12 are more pronounced.
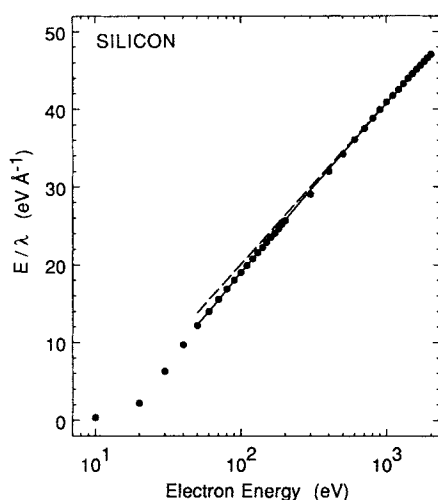
We have made least-squares fits of Eqn. (2) to our calculated IMFPs over the 50–2000 eV energy range. Examples of the quality of these fits are shown by the solid lines in Figs 1–10. The solid lines in the Fano plots (Figs 11 and 12) also indicate these fits, while the dashed lines show only the leading term of Eqn. (2), which dominates for energies above 1000 eV. The RMS deviation in the fits varied between 0.1 and 1%; the maximum deviation at any one energy was 2.5%.

Table 3 shows values of the parameters β, γ, C and D found in the least-squares fits. It should be noted that the values of β and γ in Table 3 are different from those derived in our previous analysis[1] of IMFPs over the 200–2000 eV range largely on account of the two additional terms in Eqn. (2). We also point out that Eqn. (2) together with the parameter values in Table 3 can be used for interpolation of the IMFP values in Table 2; that is, Eqn. (2) provides an explicit dependence of IMFP on energy for the 27 elements considered here.

Development of a predictive IMFP formula

We previously developed a predictive IMFP formula based on Eqn. (1) from our IMFP calculations for 27 elements and four compounds in the 200–2000 eV energy range.[1] We sought relationships of the values of β and γ for each material in terms of various material parameters (number of valence electrons per atom or molecule, bulk density, atomic or molecular weight and band-gap energy for non-conductors). We were guided

Figure 11. Fano plot for Si in which values of E/λ (solid circles) are plotted versus electron energy on a logarithmic scale. The solid line is a plot of E/λ based on the fit of Eqn. (2) to the calculated IMFP values. The dashed line shows E/λ from the first term of Eqn. (2), i.e. the Bethe equation (Eqn. (1)).
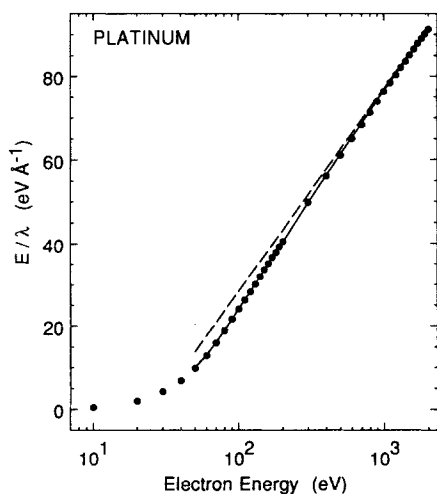

Figure 12. Fano plot for Pt; see caption to Fig. 11.

Table 3. Values of β, γ, C and D found in the fits of the modified Bethe equation (Eqn. (2)) to the calculated IMFPs over the 50–2000 eV energy range (Table 2)

Element	β (eV^{-1} Å^{-1})	γ (eV^{-1})	C (Å^{-1})	D (eV Å^{-1})
C	0.0159	0.117	0.905	18.4
Mg	0.0661	0.143	3.11	101.0
Al	0.0451	0.0951	0.852	25.4
Si	0.0329	0.0919	0.543	13.3
Ti	0.0291	0.122	1.21	18.5
V	0.0206	0.107	1.02	23.9
Cr	0.0196	0.0932	1.36	33.4
Fe	0.0155	0.0742	0.991	30.4
Ni	0.0137	0.0519	0.792	27.7
Cu	0.0127	0.0439	0.513	20.6
Y	0.0753	0.0975	3.22	64.3
Zr	0.0451	0.0977	1.91	38.1
Nb	0.0283	0.0624	0.990	22.8
Mo	0.0273	0.0706	1.43	31.5
Ru	0.0188	0.0814	1.37	33.5
Rh	0.0186	0.0758	1.43	38.5
Pd	0.0142	0.0648	0.567	14.2
Ag	0.0200	0.0574	1.69	54.8
Hf	0.0510	0.0351	0.024	15.6
Ta	0.0481	0.0404	1.51	59.0
W	0.0396	0.0383	1.04	35.0
Re	0.0386	0.0388	1.78	62.2
Os	0.0281	0.0343	0.818	32.2
Ir	0.0237	0.0347	0.494	19.1
Pt	0.0232	0.0384	0.751	27.1
Au	0.0235	0.0424	1.57	55.7
Bi	0.0624	0.0637	3.28	115.9

by relationships deduced in previous studies[26] and looked for expressions to represent any remaining residuals. IMFP values from the predictive formula (which we now call TPP-1) were compared to the IMFPs calculated for each of the 31 materials and we found an average RMS difference of 12% and a maximum RMS difference of 32%. These differences were not considered excessive in view of uncertainties in the optical data used in the calculations and the empirical basis of our formula.

We have performed a similar analysis based on the IMFP calculations for the group of 27 elements. We started with similar expressions for the Bethe parameters β and γ and then searched for useful expressions for C and D. Our results are as follows[5]

$$\beta = -0.0216 + 0.944/(E_p^2 + E_g^2)^{1/2} + 7.39 \times 10^{-4}\rho \quad (3a)$$

$$\gamma = 0.191\rho^{-0.50} \quad (3b)$$

$$C = 1.97 - 0.91U \quad (3c)$$

$$D = 53.4 - 20.8U \quad (3d)$$

$$U = N_v\rho/M \quad (3e)$$

where E_g is the band-gap energy (in eV) for nonconductors. We will refer to Eqns (2) and (3) as TPP-2.

Figure 13 shows a plot of the values of β (solid circles) found for each element (Table 3) from the fits of Eqn. (2) to the calculated IMFPs versus $(E_p^2 + E_g^2)^{-1/2}$. This plot shows a reasonably linear relationship between these variables. The dashed line in Fig. 13 is a plot of the first two terms of Eqn. (3a) versus $(E_p^2 + E_g^2)^{-1/2}$. We found that the residuals defined by

$$\beta_r = \beta + 0.0216 - 0.944/(E_p^2 + E_g^2)^{1/2} \quad (4)$$

were not random but showed a linear dependence on density, as indicated in Fig. 14. The solid line in Fig. 14 shows the explicit dependence on density indicated by the third term of Eqn. (3a). An evaluation of Eqn. (3a) for a hypothetical material with $\rho = 10$ g cm^{-3} is shown as the solid line in Fig. 13 to illustrate the magnitude of the density term in the evaluation of β.
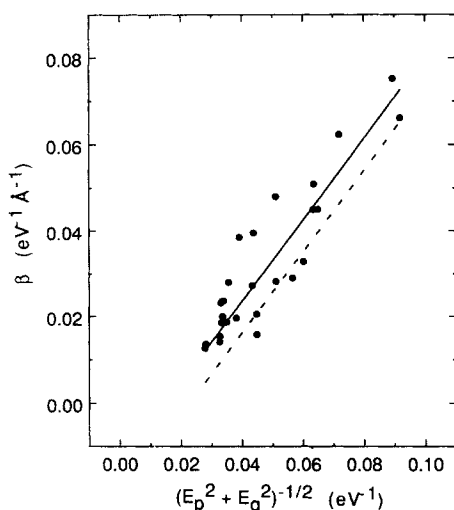

Figure 14. Plot of β_r defined by Eqn. (4) as a function of density ρ. The solid line shows the line $\beta_r = 7.39 \times 10^{-4}\rho$.

Figure 15 shows a plot of the values of γ found for each element versus density. The solid line is a plot of Eqn. (3b), which provides a good representation of the density dependence.

Figures 16 and 17 show plots of the values of C and D for each element together with Eqns 3(c) and 3(d), respectively, versus U (Eqn. 3(e)). At first glance, it seems that there are significant outliers in each figure, particularly for low values of U. This result is due to the fact that the values of C and D can be highly correlated when the Fano plots do not exhibit significant curvature at low energies. The Fano plot for Si in Fig. 11 shows less curvature at low energies than that for Pt in Fig. 12 and, as a result, the derived values of C and D are highly correlated and cannot be determined with high relative precision.

The most significant outliers in Figs 16 and 17 are the points for Mg, Al, Si, Hf and Bi. To analyse these results further, we have calculated the slopes of the Fano plots and these are shown in Figs 18 and 19. The solid circles in these plots are numerical evaluations of $d(E/\lambda)/d(\ln E)$ from our IMFP calculations. The solid lines are

Figure 13. Values of β (solid circles) found for each element (Table 3) from the fits of Eqn. (2) to the calculated IMFPs (Table 2) plotted versus $(E_p^2 + E_g^2)^{-1/2}$. The dashed line is a plot of $[0.944(E_p^2 + E_g^2)^{-1/2} - 0.0216]$ while the solid line shows a plot of Eqn. (3a) for $\rho = 10$ g cm^{-3}.
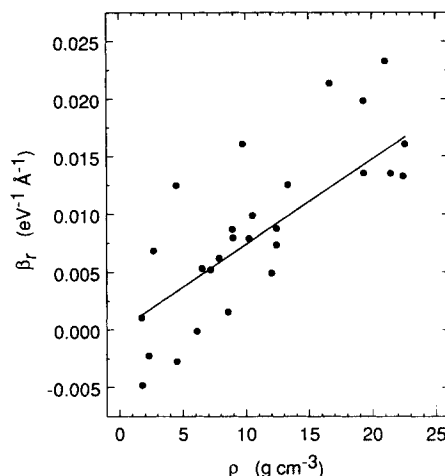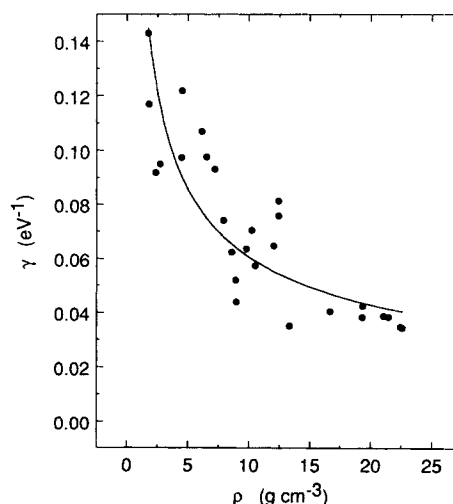

Figure 15. Values of γ (solid circles) found for each element (Table 3) from the fits of Eqn. (2) to the calculated IMFPs (Table 2) plotted versus density ρ. The solid line is a plot of Eqn. 3(b).
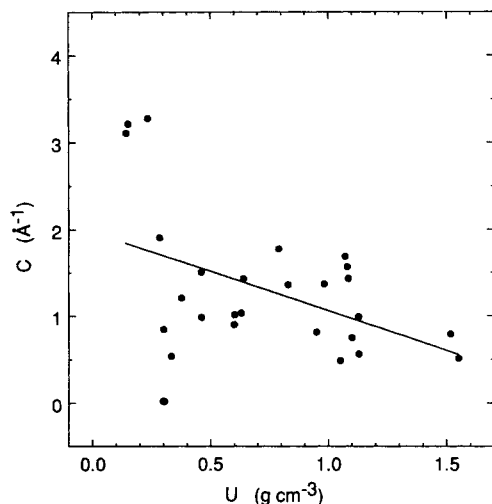
Figure 16. Values of C (solid circles) found for each element (Table 3) plotted versus U (Eqn. 3(e)). The solid line is a plot of Eqn. 3(c).
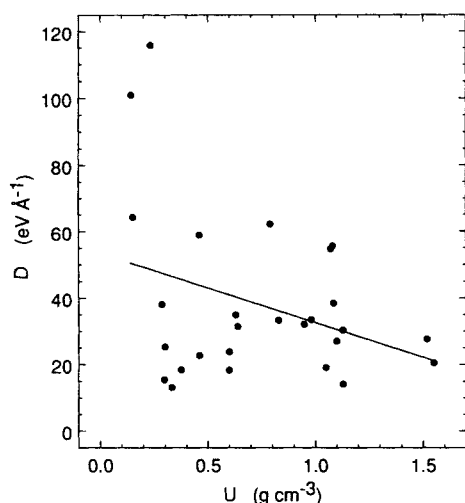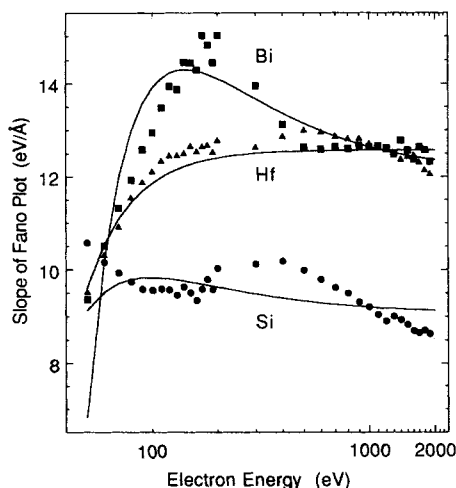

Figure 19. Slopes of Fano plots for Mg (■) and Al (●) as a function of electron energy; see caption to Fig. 18.

Figure 17. Values of D (solid circles) found for each element (Table 3) plotted versus U (Eqn. 3(e)). The solid line is a plot of Eqn. 3(d).

Figure 18. Plots of the slopes of the Fano plots $(\mathrm{d}(E/\lambda)/\mathrm{d}(\ln E))$ from the calculated IMFPs for Si (●), Hf (▲) and Bi (■) as a function of electron energy. The solid lines indicate the slopes calculated from Eqn. (5) with parameters from Table 3 for each element to show the slopes derived from the fits of Eqn. (2) to the IMFP values of Table 2.
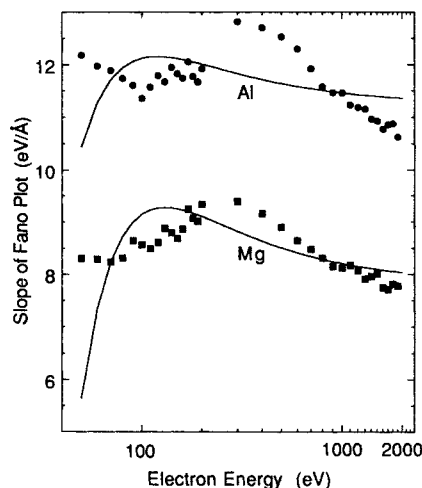
evaluations for each element of the Fano plot slopes expected from Eqn. (2), i.e. we have evaluated

$$\frac{\mathrm{d}(E/\lambda)}{\mathrm{d}(\ln E)} = E_\mathrm{p}^2\left(\beta + \frac{C}{E} - \frac{2D}{E^2}\right) \qquad (5)$$

using the parameter values listed in Table 3. For the three elements which are most free-electron-like (Mg, Al and Si), the Fano plot slopes calculated from the IMFP data do not change appreciably with electron energy. A larger variation in the Fano plot slopes with energy is found for Hf and Bi, which have a structure due both to plasmon excitation and to shallow core-level excitation in their energy-loss spectra (equivalently, the plots of $Im[-1/\varepsilon(\hbar\omega)]$ versus $\hbar\omega$). The differences from element to element in Figs 18 and 19 are largely associated with differences in the energy-loss spectra, as are the differences in the Fano plots of Figs 11 and 12. We note also that Eqn. (2) does not provide a good representation of the Fano plot slope trends for Mg, Al and Si at the lowest energies (50–60 eV) in Figs 18 and 19, although the fits of Eqn. (2) to the calculated IMFPs (e.g. Fig. 2) are satisfactory. At the highest energies (1000–2000 eV), Figs 18 and 19 show the expected asymptotic trend towards the slope expected from the Bethe equation (Eqn. (2)).[1] It therefore appears that the scatter of points in Figs. 16 and 17 for low values of U is due in part to correlation in the values of C and D in the least-squares fits, as mentioned earlier, and also in part to differences in the electron energy-loss spectra for each element. The solid lines in Figs 16 and 17 provide a reasonable means of minimizing the effects of correlations but cannot adequately represent differences in the details of the inelastic scattering for each material.

To evaluate the reliability of Eqns (2) and (3) for predicting IMFPs, we show calculated IMFPs as dashed lines in Figs 1–10 for which values of the four parameters in Eqn. (3) have been computed from property data for each element. We also list in Table 4 values for the largest positive percentage difference and the largest negative percentage difference for each element in comparisons of the results of Eqns (2) and (3) with the original IMFP values (Table 2); also shown are the electron energies at which the designated differences occur. The final column in Table 4 gives values of the root mean

Table 4. Values of the largest negative percentage difference, the largest positive percentage difference and the root mean square (RMS) percentage difference found for each element in comparing IMFP results from the predictive formula TPP-2 (Eqns (2) and (3)) with the IMFP results shown in Table 2[a]

Element	Largest positive diff. (%)	E_{pos} (eV)	Largest negative diff. (%)	E_{neg} (eV)	RMS diff. (%)
C	—	—	−45	50	−33
Mg	—	—	−7	50	−4
Al	14	60	—	—	9
Si	—	—	−18	300	−16
Ti	—	—	−12	2000	−9
V	8	50	−13	2000	−9
Cr	13	70	—	—	8
Fe	11	60	—	—	6
Ni	12	1600	−22	50	10
Cu	3	2000	−25	50	−9
Y	16	200	−4	50	14
Zr	14	110	—	—	11
Nb	—	—	−15	50	−14
Mo	11	130	—	—	8
Ru	6	100	−1	2000	4
Rh	9	300	−1	50	6
Pd	—	—	−18	1500	15
Ag	11	2000	−23	50	10
Hf	11	50	−6	300	−4
Ta	37	50	—	—	20
W	30	50	—	—	15
Re	23	2000	—	—	20
Os	2	50	−8	120	−7
Ir	—	—	−16	500	−14
Pt	—	—	−11	500	−11
Au	—	—	−27	50	−13
Bi	19	50	—	—	15

[a] The sign of the difference indicates whether the values from TPP-2 are systematically lower (−) or higher (+) than the values of Table 2. E_{pos} and E_{neg} are the energies at which the largest positive and negative differences, respectively, occur.

square (RMS) difference between the IMFP results from Eqns (2) and (3) and the values of Table 2.

Figures 1–10 provide a visual indication of the extent to which results from our predictive formula TPP-2 agree with the directly calculated IMFP values. A more quantitative comparison can be made from the information in Table 4. For about half of the elements, the largest percentage differences (positive or negative) occur at the lowest electron energy considered here (50 eV) while for about a quarter of the elements the largest differences occur at the highest energy (2000 eV). The differences are entirely positive or negative for two-thirds of the elements while for the remainder both positive and negative differences are found. The largest negative percentage difference is for carbon (−45% at 50 eV) and the largest positive percentage difference is for tantalum (37% at 50 eV). A reasonable overall comparison can be made using values for the RMS differences listed in the final column of Table 4; this is a reasonable basis for evaluation even though the differences are systematic rather than random. The largest RMS difference is for carbon (−33%) and the average RMS difference is ∼13%. This value for the average

RMS difference compares favourably with the corresponding value of 12% in the similar evaluation of TPP-1 over the 200–2000 eV range.[1] We believe that the differences shown in Table 4 are not unreasonable considering the uncertainties of the optical data used in the IMFP calculation[1] and the empirical basis of the modifications to the Bethe equation and of the four parameters of Eqn. (2) given in Eqn. (3). As discussed further below, Eqns (2) and (3) can only be expected to be an approximate guide to the very different inelastic electron scattering behavior of the various solids.

With only one semiconductor in our group of 27 elements, it has not been possible here to validate the inclusion of the E_g term in Eqn. (3a). We show in the following paper[6] that this small correction in Eqn. 3(a), as suggested by Szajman et al.,[26] is useful.

DISCUSSION

Comparisons of IMFP values with other results

Two other groups[14,27] have calculated IMFP values from optical data in a similar manner to that done here. Ashley[14] has calculated IMFPs for Al, Cu, Ag and Au both with and without consideration of exchange although, as pointed out earlier, his treatment of exchange is approximate. Exchange effects are larger for smaller electron energies and, at the lowest energy of 40 eV for which numerical values are reported, Ashley finds that exchange leads to increases of the calculated IMFPs for Al, Cu, Ag and Au by between 28 and 40%.

Ding and Shimizu[27] have calculated IMFPs for Si, Ni, Cu, Ag and Au using two different dispersion equations that relate excitation energy to momentum transfer. With a quartic equation relating excitation energy to momentum transfer q (as used here), they find reductions in the calculated IMFP values compared to those found with a quadratic equation (as used by Ashley). The reductions are only significant for energies below 200 eV; at an energy of 50 eV, the reductions range from ∼20% for Si to 45% for Au.

While these differences in technical approach led to up to 50% differences in numerical IMFP values for electron energies between 50 and 200 eV, there is much closer agreement in the results for higher energies. At an energy of 1000 eV, for example, the IMFP values calculated for Au by us and those reported in Refs 14 and 25 differ by a maximum of 11%; the corresponding difference for Cu is also 11%.

Reich et al.[28] have calculated IMFPs using an atomic model. Although the detailed inelastic scattering mechanisms for valence electron excitations, particularly in atoms and the corresponding solids, are quite different, the atomic model yields results that are in semi-quantitative agreement with other data.[28] This result is not surprising since the total oscillator strengths for valence electron excitations from atoms and from those atoms in an elemental solid will be similar even if the excitation modes and energies are different. Nevertheless, the IMFPs calculated by Reich et al. for C, Al and Si from their atomic model are typically 20–40% lower than the values that we determined for those solids (Table 2).

We have previously[1] compared our IMFP values in the 200–2000 eV range with experimental measurements of electron attenuation lengths (ALs) and found semi-quantitative agreement. Owing to elastic electron scattering, IMFP values will be systematically larger than corresponding AL values by up to ~40%, depending on the electron energy, the atomic number of the material and the experimental configuration.[29] The experimental AL measurements may have uncertainties of up to a factor of approximately two owing to a large number of sources of systematic error.[17,30] It is therefore difficult at this time to draw useful conclusions from IMFP and AL values which appear either to agree or to disagree.

The IMFP predictive formula TPP-2

Equations (2) and (3) are believed to be useful for predicting IMFP values for materials for which no calculations or measurements have been made. Since we have used the same algorithm in our IMFP calculations for the present group of 27 elements, we consider that these equations (TPP-2) can provide information on the dependence of the IMFP on energy and material even though the absolute values may be systematically high or low on account of the approximations adopted in the theory.[2]

Nevertheless, we point out some limitations of TPP-2. In addition to the uncertainties associated with the theory, the IMFP values calculated for optical data for any one material will have an additional uncertainty of ~10% associated with the typical uncertainty of the optical data for these 27 materials, as noted earlier. The scatter of points in Figs 13–17 is believed to be due in part to uncertainties of the optical data.

Another limitation of TPP-2 is associated with the empirical nature of Eans (2) and (3). A simple analytical description such as this cannot be expected to represent adequately the detailed differences in inelastic scattering from element to element. For example, we show in Figs 20 and 21 plots of the energy-loss functions for Si and Pt as examples of the qualitatively different distributions found for so-called free-electron and non-free-elec-
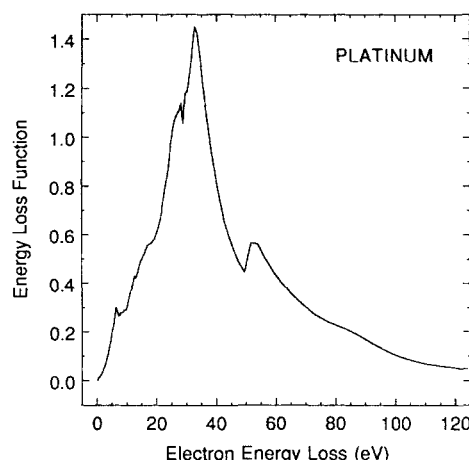
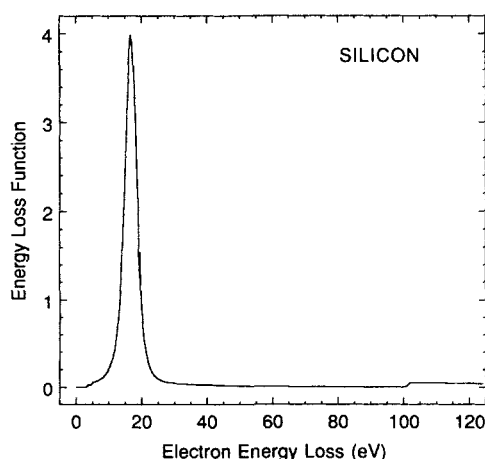**Figure 21.** Plot of the electron energy-loss function for Pt, $Im[-1/\varepsilon(\omega)]$, as a function of energy loss $\hbar\omega$ (Ref. 11).

tron materials, respectively.[31] The energy-loss function is proportional to the differential cross-section for inelastic scattering as a function of energy loss.[31] For Si, as shown in Fig. 20, the most probably energy loss is at 16.6 eV and is due to bulk plasmon excitation. The additional weaker structure at ~100 eV energy loss corresponds to the onset of excitations from the L shell. In contrast, the energy-loss function for Pt in Fig. 21 shows much broader structures that overlap. For most transition and noble metals, it is not possible to identify unequivocally the structures due to bulk plasmon and to single electron excitations.[32] There are also overlaps in the structures due to valence electron and core electron excitation. Despite the range and complexity of the structures found for valence electron excitations (generally those for which the excitation energy is < 50 eV), an IMFP calculated from the optical data for a given material and electron energy results from an integration of all available excitations. The effects of differences in the spectrum of inelastic excitations from one material to another can thus be reduced by this integration. The averaging of material differences will, however, generally be less at low electron energies (< 200 eV) since the relative cross-sections for the various inelastic channels at different excitation energies become more sensitive functions of electron energy. The effects of differences in inelastic scattering from material to material are therefore likely to be more pronounced at such low energies. These effects cannot be accurately represented by the relatively simple formula TPP-2, as we will show later in this subsection.

A final aspect of TPP-2 is the sensitivity of the computed IMFPs to the choice of parameters, particularly the number N_v of valence electrons per atom or molecule. This issue is addressed further below but here we point out that this parameter arises from sum-rule considerations[31] and not the position of a plasmon-loss peak in the energy-loss function, which depends on other parameters.[32]

The magnitude of the IMFP for a given material is inversely related to the total cross-section for inelastic electron scattering and to the density of atoms or molecules. Most of the total inelastic scattering cross-section for electron energies of interest in AES and XPS is due to valence electron excitations with energies

Figure 20. Plot of the electron energy-loss function for Si, $Im[-1/\varepsilon(\omega)]$, as a function of energy loss $\hbar\omega$, as calculated from optical data (Ref. 11).

typically between 5 and 50 eV, as illustrated in Figs 20 and 21. The magnitude of the cross-section for valence electron excitations can be estimated from the most probable excitation energy and the valence electron oscillator strength.[31] Such oscillator strengths can be determined from an evaluation of the integral

$$Z_{eff} = \left(\frac{2}{\pi\hbar^2\Omega_p{}^2}\right) \int_0^{\Delta E_{max}} \Delta E \, Im\left[-\frac{1}{\varepsilon(\Delta E)}\right] d(\Delta E) \quad (6)$$

where $\Omega_p = (4\pi n_a e^2/m)^{1/2}$, $n_a \rho/M$ is the density of atoms or molecules, N_a is Avogadro's number, ρ is the bulk density, M is the atomic or molecular weight and $\Delta E = \hbar\omega$ is the energy loss in an inelastic scattering event corresponding to the photon energy $\hbar\omega$. Estimates of the valence electron oscillator strength are typically made by choosing the upper limit in Eqn. (6), ΔE_{max}, to be less than the binding energy of the shallowest core electrons.

When the upper limit in Eqn. (6) (ΔE_{max}) is equal to infinity, Z_{eff} should be equal to Z, the total number of electrons per atom or molecule.[33] In this limit, Eqn. (6) is the oscillator strength (f-sum) rule. Unfortunately, there is no 'partial' sum rule associated with each electronic shell, although it is found empirically that Z_{eff} evaluated with $\Delta E_{max} = 50{-}100$ eV is often equal to the number of valence electrons per atom or molecule within $\sim 20\%$.

We show examples of evaluations of Z_{eff} as a function of ΔE_{max} in Figs 22 and 23 for Si and Pt, respectively. These two elements have very different energy-loss functions (Figs 20 and 21) and there are corresponding differences in Figs 22 and 23. Figure 22 for Si shows three reasonably well-defined plateaux that define regions predominantly associated with valence electron, L-shell and K-shell excitations. Even for this relatively ideal case, it is clear that there are valence electron excitations with energies greater than the L_3-subshell binding energy and there are L-shell excitations with energies greater than the K-shell binding energy. In contrast, Fig. 23 for Pt does not show plateaux as in Fig. 22 and it is evident here, as for other transition and noble metals, that there is a much greater
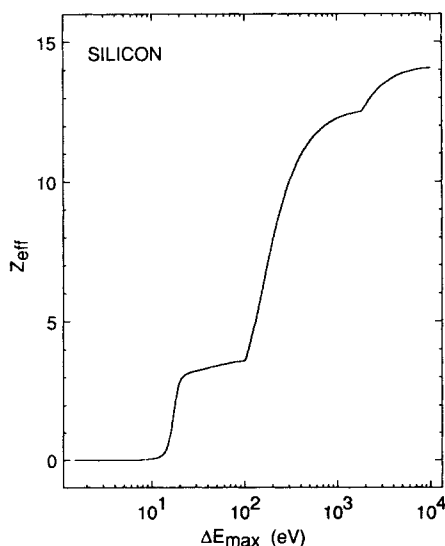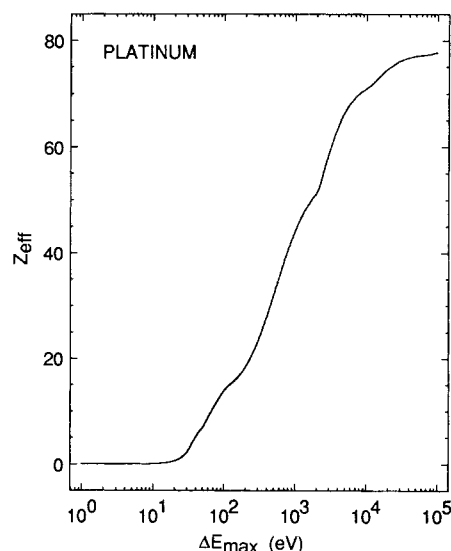

Figure 23. Plot of Z_{eff} versus ΔE_{max} from Eqn. (6) for Pt.

overlap in the excitations for the various shells. The valence electron excitations of Pt, for example, overlap excitations of the O_{23} subshells with an onset at ~ 50 eV. Despite these various complications, the total number of valence electrons (four for Si and ten for Pt) provides an initial estimate, through the parameter E_p in Eqn. (2), of the oscillator strength for valence electron excitations that provide the largest contribution to the total inelastic scattering cross-section. That this estimate is in fact generally reasonable is shown by the RMS differences in Table 4 in the comparisons of IMFP values from TPP-2 with our calculated IMFPs.

There are also some elements such as zinc where there are core levels with very low binding energy, in this case ~ 10 eV. The latter electrons have excitations which clearly contribute to the total inelastic scattering cross-section. In such cases, it is suggested that an IMFP value be calculated from TPP-2 using the number of valence electrons per atom as a reasonable estimate; in addition, it is suggested that the calculation be repeated including the core electrons to give an upper limit for the uncertainty due to this parameter. The IMFP calculated for Zn at $E = 1000$ eV from TPP-2 for $N_v = 2$ is 24.2 Å, while the value for $N_v = 12$ is 17.8 Å, a reduction of 26%. Although this uncertainty of 26% in the calculated IMFP is substantial, it nevertheless corresponds to a factor of six variation in the value of the parameter N_v. The effects of varying the values of the parameters in TPP-2 on the predicted IMFP are discussed in more detail in the following subsection.

We have discussed in some detail the limitations of TPP-2 for predicting absolute IMFPs. Relative IMFPs, however, can be obtained with greater confidence. Figure 24 shows a plot of the ratios of IMFPs calculated from TPP-2 to the IMFPs calculated from optical data for Al, Au, Pt and Si as a function of electron energy. For energies above 200 eV, this ratio is constant to within 2% for Al, 6% for Au, 1% for Pt and 2% for Si. The ratio is constant for the group of elements to within an average value of 4% and a standard deviation of 2.4% over the 200–2000 eV energy range. At lower
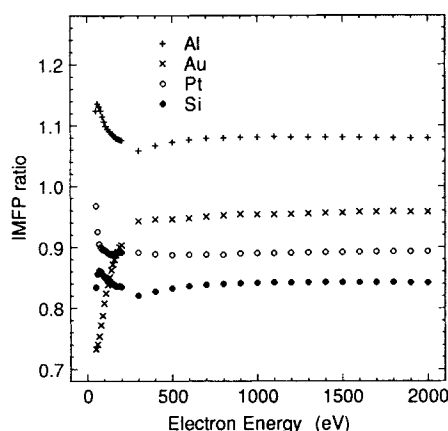

Figure 22. Plot of Z_{eff} versus ΔE_{max} from Eqn. (6) for Si.

Figure 24. Plot of the ratios of IMFPs calculated from TPP-2 to the IMFPs calculated from optical data for Al, Au, Pt and Si as a function of electron energy.

Table 5. Parameter values for Al and Au needed for evaluation of the IMFP predictive formula TPP-2 (Eqns (2) and (3))

Parameter	Al	Au
ρ (g cm^{-3})	2.7	19.3
N_v (electrons per atom)	3	11
E_p (eV)	15.8	29.9
U (g cm^{-3})	0.300	1.079
β(eV^{-1} Å^{-1})	0.0402	0.0242
γ (eV^{-1})	0.116	0.04435
C (Å^{-1})	1.70	0.988
D (eV Å^{-1})	7.2	31.0

energies, however, the ratio could show larger variations, as exemplified by the maximum variation of 24% found for Au. This large change in the IMFP ratio for Au at low energies illustrates a limitation of the TPP-2 formula that was discussed earlier.

We have also found that the average RMS difference between IMFPs calculated from the optical data and the values predicted by TPP-2 over the 50–2000 eV range for the group of 27 elements was ~13%. This average RMS difference indicates the precision with which relative IMFP values can be obtained from TPP-2 for different materials at a given energy. This precision is almost a factor of three less than that found with the widely used Seah and Dench formula for predicting electron attenuation lengths in elemental solids.[35]

We note, finally, here that when we initially developed and published[4,5] a predictive formula for the 50–2000 eV energy range, we gave different expressions for the parameters C and D. We were informed[34] that these expressions led to non-physical IMFP values for certain parameter choices. We later developed[5] simpler expressions for C and D which do not give the same problems; our analyses which led to these expressions and to our TPP-2 formula have been described above. We emphasize that our IMFP calculations were made for electron energies between 50 and 2000 eV and for a group of elements that have values for the parameter U ranging between 0.14 and 1.55. We strongly recommend that our predictive formula TPP-2 not be used for energies and for materials with values of U outside these ranges, i.e. TPP-2 should only be used for interpolation purposes over the ranges of variables considered here.

Characteristics of the predictive formula TPP-2

We pointed out earlier[5] the substantial differences in the shapes of the IMFP versus energy curves for Al and Au between 50 and 200 eV. Our formula TPP-2 appears to represent reasonably the various IMFP versus energy curves at such low energies for Al and Au as well as for the other elements analysed here (see, for example, Figs 1–10 and Table 4). We therefore thought it worthwhile to examine in greater detail the influence

of the various parameters in TPP-2 on the IMFP magnitudes and on the shapes of the IMFP versus energy curves.

We have chosen to evaluate TPP-2 for both Al and Au and then to calculate IMFP values, as each parameter in TPP-2 was separately varied. The elements Al and Au were chosen for this purpose since they are perhaps the most extreme examples of free-electron-like and non-free-electron-like metals (so far as their IMFP properties are concerned).[5] Material properties and parameters for elemental Al and Au are listed in Table 5. We note here that we have varied the parameters in TPP-2 over a substantial range and this has caused the calculated values of U to lie outside the recommended range of 0.14–1.55; the lowest value of U examined is 0.03 (corresponding to $E_p = 5$ eV), while the highest value is 2.22 (corresponding to $\rho = 20$ g cm^{-3} for Al).

Figures 25–28 show IMFP versus energy curves for Al and the effects of varying in turn the bulk density ρ, the number of valence electrons per atom N_v, the free-electron plasmon energy E_p and the band-gap energy E_g. The bulk density affects values of E_p and U and thus the parameters β, C and D as well as the value of γ.
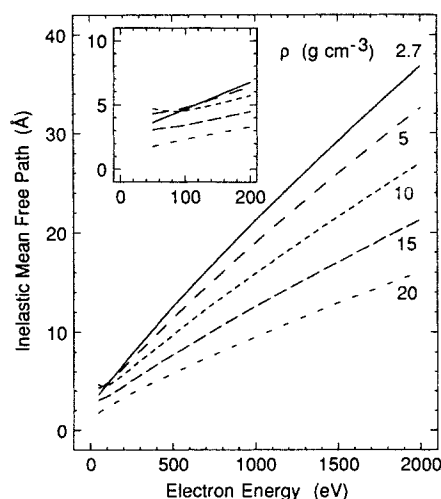

Figure 25. Plots of IMFP versus energy for Al from TPP-2 (solid line) and of evaluations of TPP-2 (Eqns (2) and (3)) with Al parameters except that the bulk density ρ was varied as shown. The inset shows IMFP values for the 50–200 eV range on an expanded energy scale.
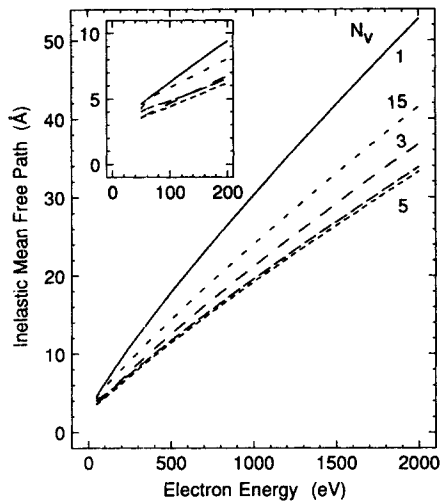
Figure 26. Plots of IMFP versus energy for Al from TPP-2 (curve with $N_v = 3$) and of evaluations of TPP-2 with Al parameters except that the number of electrons per atom N_v was varied as shown. The curve adjacent to the bottom $N_v = 5$ curve is for $N_v = 10$.

Figure 28. Plots of IMFP versus energy for Al from TPP-2 (solid curve) and of evaluations of TPP-2 with Al parameters except that the band-gap energy E_g was varied as shown. The curve adjacent to the curve for Al with $E_g = 0$ is for $E_g = 3$ eV.

Figure 25 shows that increases in the value of ρ lead to a systematic decrease of the IMFPs calculated from TPP-2 except for energies below 100 eV. In this low-energy range, changes in shape of the IMFP versus energy curves are observed. The value of N_v determines values of E_p and U and consequently of β, C and D. Variation of N_v from 1 to 5 leads to a decrease in IMFP values, as shown in Fig. 26, but further increase of N_v causes increases of the IMFPs. Figure 27 shows the effects of varying the parameter E_p (and consequently also U). An increase of E_p from 5 eV to 25 eV decreases the IMFP for energies greater than 100 eV, but increases of E_p to 30 and 35 eV lead to increases of the IMFP. For energies below 100 eV, changes of E_p cause some changes in the shapes of the IMFP versus energy curves. Although Al is, of course, a metal and the band-gap energy $E_g = 0$, we show in Fig. 28 how variation of this parameter affects the calculated IMFPs. Increase of
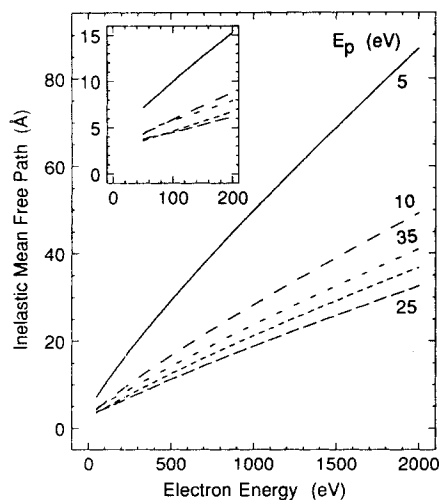
E_g leads to a decrease of β and an increase in the computed IMFP as illustrated.

Figures 29–32 show similar plots for Au. Variation of the value of the bulk density, as shown in Fig. 29, causes a similar variation in IMFP magnitudes as shown in Fig. 25, although the Au curves at low energies (the inset of Fig. 29) show a broad minimum for the larger densities. Figure 30 shows the effects of changing the value of N_v. There is here a systematic variation of the IMFP with N_v in contrast to the more complex trends found for Al in Fig. 26. The IMFP versus energy curves in the inset of Fig. 30 all display a broad minimum. An increase in the value of E_p causes a systematic decrease in IMFP values, as shown in Fig. 31. There are also substantial changes in the shapes of the IMFP versus energy curves for energies below 200 eV; for $E_p = 35$ eV the IMFP does not vary substantially between 50 and 200 eV, while for $E_p = 5$ eV the IMFP

Figure 27 Plots of IMFP versus energy for Al (with $E_p = 15.8$ eV) from TPP-2 (curve adjacent to the bottom curve) and of evaluations of TPP-2 with Al parameters except that the free-electron plasmon energy E_p was varied as shown.
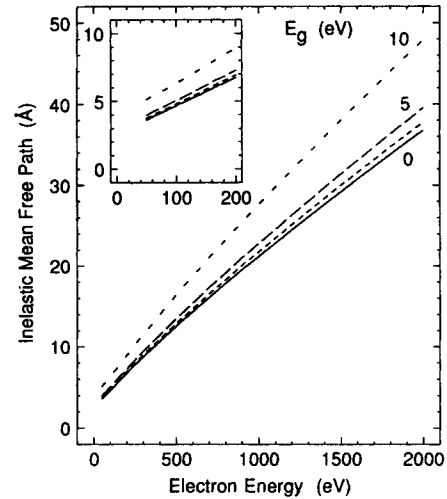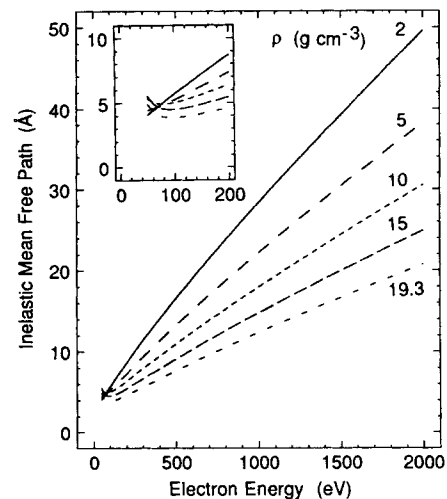

Figure 29. Plots of IMFP versus energy for Au from TPP-2 (lowest curve) and of evaluations of TPP-2 with Au parameters except that the bulk density ρ was varied as indicated.
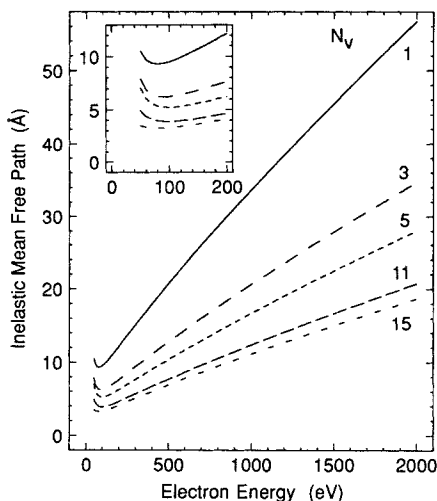
Figure 30. Plots of IMFP versus energy for Au from TPP-2 (curve with $N_v = 11$) and of evaluations of TPP-2 with Au parameters except that the number of electrons per atom N_v was varied as shown.
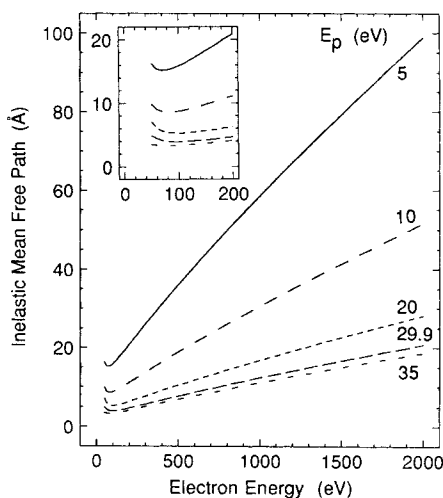

Figure 31. Plots of IMFP versus energy for Au from TPP-2 (curve with $E_p = 29.9$ eV) and of evaluations of TPP-2 with Au parameters except that the free-electron plasmon energy E_p was varied as shown.
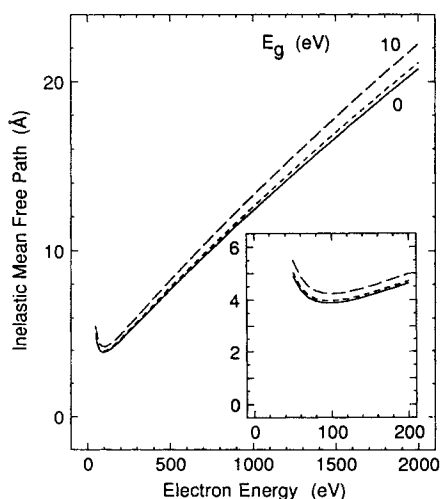

Figure 32. Plots of IMFP versus energy for Au from TPP-2 (solid line) and of evaluations of TPP-2 with Au parameters except that the band-gap energy E_g was varied. The intermediate curve is for $E_g = 5$ eV.

variation is greater. Finally, we show in Fig. 32 the effects of varying the magnitude of E_g. As expected from Eqn. (3a), an increase of E_g for a material such as Au with $E_p = 29.9$ eV is smaller than in the case of Al (Fig. 28) where $E_p = 15.8$ eV.

The plots of Figs 25–32 illustrate the sensitivity of the calculated IMFPs and the shapes of the IMFP versus energy curves to variations in the values of individual parameters. Figures 26 and 30, in particular, show how changes in the choice of N_v affect the IMFP values for Al and Au when other parameters are held constant. The value of E_p affects the magnitude of the IMFP, as shown in Figs 27 and 31, and also the shapes of the IMFP versus energy curves for low energies in Fig. 31.

The parametric calculations reported in Figs 25–32 give an insight into how TPP-2 is able to represent the different shapes of the IMFP versus energy curves of Al and Au in the 50–200 eV energy range. For almost all values of the parameters selected in Figs 25–28, the IMFP increased with increasing energy and the expected minimum presumably occurred below 50 eV (as it does in elemental Al[5]). Figures 29–32 show a broad minimum at low energies except when the values of ρ, N_v and E_p are reduced from the values for Au. The broad minima in the IMFP versus energy curves that are characteristic of the transition and noble metals are therefore associated in TPP-2 with higher values of ρ, N_v and E_p than are typical for the more free-electron-like elements (such as Mg, Al and Si).

Use of the predictive formula TPP-2

IMFPs can be calculated from TPP-2 for a given material using appropriate values of bulk density and atomic or molecular weight that have been tabulated in handbooks.[36] Information on sources for the band-gap energy of non-conductors is presented in the following paper.[6] The choice of a value for N_v can be complex for some materials, as discussed in the previous two subsections, but we give examples of choices for this parameter in Refs 1 and 6.

Shapes of the IMFP versus energy curves

The shapes of the IMFP versus energy curves for energies below 200 eV differ from element to element (for example, Figs 1–10). These differences are believed to be associated with the different shapes of the energy-loss functions for each material.[5] The differential inelastic scattering cross-section with respect to energy loss is proportional to the energy-loss function.[31] The shape of the IMFP versus energy curve at energies below 200 eV is largely determined by integration over the available inelastic scattering channels with weightings determined by the energy-loss function. Our use of experimental optical data ensures that we use the appropriate weighting distribution for each material.

The energy at which the IMFP is a minimum also varies substantially from element to element. The smallest such energy is 30 eV (for Mg) and the largest is 125 eV (for Au). The energy for the minimum IMFP is plotted versus free-electron plasmon energy in Fig. 33
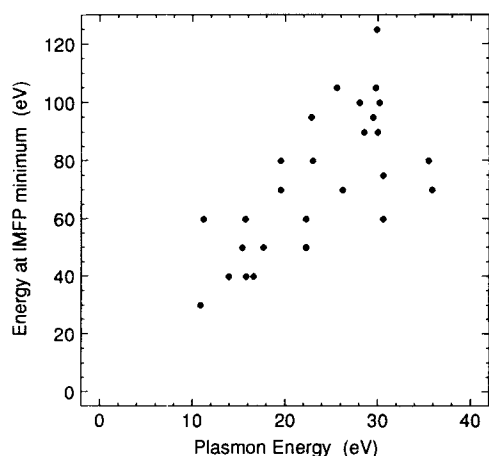
Figure 33. Plot of the electron energy for which the calculated IMFP of an element (Table 2) is a minimum versus the free-electron plasmon energy (Table 1) for the group of 27 elements.

and, while the data are scattered, it can be seen that there is an approximate linear dependence. Such a dependence is expected from early IMFP calculations[37] for jellium, a fictitious material of variable electron density. The same theory predicts that the minimum IMFP should be independent of plasmon energy (and also of electron density). We find that the minimum IMFP (Table 2) varies from 3.11 Å (Al) to 5.78 Å (C), although for 21 out of the 27 elements the minimum IMFPs range between 4.08 Å and 4.98 Å.

The dominant form of inelastic electron scattering in jellium is plasmon excitation and we therefore do not expect the jellium theory to be a reliable guide to the inelastic scattering behaviour of transition and noble metals, for the reasons discussed earlier in connection with Figs 20 and 21. Nevertheless, the jellium theory does provide a semi-quantitative guide to the observed trends. We attribute the scatter in Fig. 33 and the range of values for the minimum IMFP to detailed differences in the shapes of the energy-loss functions for our group of 27 elements. We also note that the empirical AL formula proposed by Seah and Dench[35] predicts minimum IMFP values between 3.47 Å (Ni) and 6.01 Å (Bi) for our group of 27 elements and that these minimum IMFPs occur at energies between 38.5 eV (Bi) and 41.6 eV (Ni).[5] The Seah and Dench formula does not adequately represent the variations in the shapes of the IMFP versus energy curves that we find for the 50–200 eV range of electron energies.

The shape of the IMFP versus energy curve and the location of the energy at which the IMFP is a minimum are important in photoemission and related experiments with synchrotron radiation in which the photon energy is 'tuned' to achieve maximum surface sensitivity. The plots of Figs 1–10 illustrate how the shapes of the IMFP versus energy curves vary from material to material at low energies; similar variations are seen in the corresponding plots for compounds.[6] While Fig. 33 indicates that the location of the energy at which the IMFP is a minimum varies substantially, it should be emphasized again that, for the transition and noble metals studied here, the IMFP versus energy curve is broader at low energies than for the free-electron-like solids and there is correspondingly less opportunity to

vary surface sensitivity over the 50–200 eV range of electron energies. Nevertheless, as pointed out by Norman and Woodruff,[38] surface sensitivity can be varied in experiments with synchrotron radiation and it is important then to make material-dependent selections of electron energies for a given purpose rather than to rely on so-called universal curves.[17]

SUMMARY

We have reported IMFP calculations for 50–2000 eV electrons in 27 elements. The accuracy of individual IMFP values for any material depends in part on the accuracy of the optical data on which the calculations are based; this uncertainty is typically 10% although it could be larger for some elements.[1] The other main source of inaccuracy is due to approximations in our algorithm. We previously estimated[1] this uncertainty to be ~10% for free-electron-like materials and for energies larger than 200 eV; the uncertainty for other materials and at lower energies is expected to be larger but its magnitude is difficult to estimate. We have used the same algorithm in a consistent way for this group of 27 elements and we therefore believe that relative IMFP values are known with greater confidence than absolute values, i.e. we believe that our IMFP results are particularly valuable for determining changes in IMFPs from material to material and for determining the IMFP dependence on electron energy.

We find substantial differences in the shapes of the IMFP versus energy curves for energies between 50 and 200 eV. These differences are attributed to detailed differences in the inelastic scattering behaviour of each material, as represented by their energy-loss function.

We have analysed the energy and material dependences of our IMFP values and find that they can be well represented by a modified form of the Bethe equation for inelastic electron scattering in matter. This equation contains four parameters which have been empirically related to atomic weight, bulk density and number of valence electrons per atom. The resulting formula (TPP-2) provides a convenient means for estimating absolute IMFP values in other materials. TPP-2 can also give relative IMFPs for an element at different energies in the 200–2000 eV range with a precision better than 3%. Over the 50–200 eV range, however, the precision could be worse owing to the fact that the simple TPP-2 formula cannot represent accurately the different inelastic scattering phenomena in different materials at low energies. Relative IMFPs for different elements at a given electron energy can be obtained from TPP-2 with a precision of ~13% over the 50–2000 eV energy range. We point out that TPP-2 should not be used for electron energies and for material parameters outside the ranges for which it has been developed and tested.

Acknowledgements

REFERENCES

1. S. Tanuma, C. J. Powell and D. R. Penn, *Surf. Interface Anal.* **11**, 577 (1988).
2. D. R. Penn, *Phys. Rev. B* **35**, 482 (1987).
3. H. Bethe, *Ann. Phys.* **5**, 325 (1930).
4. S. Tanuma, C. J. Powell and D. R. Penn, *J. Electron Spectrosc.* **52**, 285 (1990).
5. S. Tanuma, C. J. Powell and D. R. Penn, *J. Vac. Sci. Technol.* **A8**, 2213 (1990).
6. S. Tanuma, C. J. Powell and D. R. Penn, *Surf. Interface Anal.* **17**, 929 (1991).
7. A Jablonski, *Surf. Interface Anal.* **15**, 559 (1990).
8. I. Lindhard and M. Scharff, *K. Dan. Vidensk. Selsk. Mat.-Fys. Medd.* **27**, No. 15 (1953); J. Lindhard, M. Scharff and H. E. Schiott, *K. Dan. Vidensk. Selsk. Mat.-Fys. Medd.* **33**, No. 14 (1963); D. Pines, *Elementary Excitations in Solids*, p. 144. W. A. Benjamin, New York (1963).
9. H.-J. Hagemann, W. Gudat and C. Kunz, Deutsches Elektronen-Synchrotron Report SR-74/7, Hamburg (1974), unpublished; H.-J. Hagemann, W. Gudat and C. Kunz, *J. Opt. Soc. Am.* **65**, 742 (1975).
10. J. H. Weaver, C. Krafta, D. W. Lynch and E. E. Koch, *Optical Properties of Metals* Physics Data Nos. 18-1 and 18.2. Fachinformationszentrum, Karlsruhe (1981).
11. *Handbook of Optical Constants of Solids*, ed. by E. D. Palik. Academic Press, New York (1985).
12. B. L. Henke, P. Lee, T. J. Tanaka, R. L. Shimabukuro and B. K. Fujikawa, in *Low Energy X-ray Diagnostics*, ed. by D. T. Attwood and B. L. Henke, p. 340, Am. Inst. Phys. Conf. Proc. No. 75. American Institute of Physics, New York (1981).
13. B. L. Henke, P. Lee, T. J. Tanaka, R. L. Shimabukuro and B. K. Fujikawa, *At. Data Nucl. Data Tables* **27**, 1 (1982).
14. J. C. Ashley, *J. Electron Spectrosc.* **46**, 199 (1988).
15. D. R. Penn, *Phys. Rev. B* **22**, 2677 (1980).
16. D. L. Abraham and H. Hopster, *Phys. Rev. Lett.* **58**, 1352 (1987); O. Paul, M. Taborelli and M. Landolt, *Surf. Sci.* **211**, 724 (1989); D. P. Pappas, K.-P. Kämper, B. P. Miller, H. Hopster, D. E. Fowler, C. R. Brundle, A. C. Luntz and Z.-X. Shen, *Phys. Rev. Lett.* **66**, 504 (1991); M. Donath, D. Scholl, H. C. Siegmann and E. Kay, *Appl. Phys.* **A52**, 206 (1991).
17. C. J. Powell, *J. Electron Spectrosc.* **47**, 197 (1988).
18. C. J. Powell, *Rev. Sci. Instrum.* **44**, 1031 (1973); S. Tougaard and I. Chorkendorff, *Phys. Rev. B* **35**, 6570 (1987); J. C. Ingram, K. W. Nebesny and J. E. Pemberton, *Appl. Surf. Sci.* **44**, 279 (1990).
19. R. H. Ritchie, *Phys. Rev.* **106**, 874 (1957); E. A. Stern and R. A. Ferrell, *Phys. Rev.* **120**, 130 (1960); C. J. Powell, *Phys. Rev.* **175**, 972 (1968).
20. V. L. Moruzzi, J. F. Janak and A. R. Williams, *Calculated Electronic Properties of Metals*. Pergamon Press, New York (1978).
21. D. A. Papaconstantopoulos, *Handbook of the Band Structure of Elemental Solids*. Plenum Press, New York (1986).
22. C. J. Powell, in *Microbeam Analysis-1990*, ed. by J. R. Michael and P. Ingram, p. 13. San Francisco Press, San Francisco, CA (1990).
23. C. J. Powell, *Surf. Interface Anal.* **10**, 349 (1987).
24. C. J. Powell, *Surf. Interface Anal.* **7**, 256 (1985).
25. M. Inokuti, *Rev. Mod. Phys.* **43**, 297 (1971).
26. J. Szajman, J. Liesegang, J. G. Jenkin and R. C. G. Leckey, *J. Electron Spectrosc.* **23**, 97 (1981); J. C. Ashley, *J. Electron Spectrosc.* **28**, 177 (1982).
27. Z.-J. Ding and R. Shimizu, *Surf. Sci.* **222**, 313 (1989).
28. T. Reich, V. G. Yarzhemski and V. I. Nefedov, *J. Electron Spectrosc.* **46**, 255 (1988).
29. A. Jablonski, *Surf. Sci.* **188**, 164 (1987); A Jablonski and H. Ebel, *Surf. Interface Anal.* **11**, 627 (1988); A. Jablonski and S. Tougaard, *J. Vac. Sci. Technol.* **A8**, 106 (1990); W. H. Gries and W. Werner, *Surf. Interface Anal.* **16**, 149 (1990); W. S. M. Werner, W. H. Gries and H. Störi, *J. Vac. Sci. Technol.* **A9**, 21 (1991); Z.-J. Ding, Ph.D. Thesis, Osaka University (1990); W. S. M. Werner, W. H. Gries and H. Störi, *Surf. Interface Anal.* **17**, 693 (1991).
30. C. J. Powell and M. P. Seah, *J. Vac. Sci. Technol.* **A8**, 735 (1990).
31. C. J. Powell, *Electron Beam Interactions with Solids for Microscopy, Microanalysis and Microlithography*, ed. by D. F. Kyser, H. Niedrig, D. E. Newbury and R. Shimizu, p. 19. Scanning Electron Microscopy, Chicago (1984).
32. C. J. Powell, *J. Opt. Soc. Am.* **59**, 738 (1969).
33. D. Y. Smith, in *Handbook of Optical Constants of Solids*, ed. by E. D. Palik, p. 35. Academic Press, New York (1985).
34. D. G. Watson, personal communication.
35. M. P. Seah and W. A. Dench, *Surf. Interface Anal.* **1**, 2 (1979).
36. *CRC Handbook of Chemistry and Physics*, ed. by R. C. Weast and D. R. Lide, p. B-68. CRC Press, Boca Raton, FL (1989/90); H. P. R. Frederikse, in *American Institute of Physics Handbook*, ed. by D. E. Gray, p. 9–16. McGraw Hill, New York (1972).
37. J. C. Shelton, *Surf. Sci.* **44**, 305 (1974).
38. D. Norman and D. P. Woodruff, *Surf. Sci.* **75**, 179 (1978).